This is a repository copy of *Magnetically Recyclable Catalytic Carbon Nanoreactors*.

White Rose Research Online URL for this paper:
http://eprints.whiterose.ac.uk/131960/

Version: Accepted Version

Magnetically Recyclable Catalytic Carbon Nanoreactors

Dr. Mehtap Aygün,[1,2] Dr. Thomas W. Chamberlain,[3] Dr. Maria del Carmen Gimenez-Lopez,[2] Prof. Andrei N. Khlobystov[1,4*]

[1]School of Chemistry, University of Nottingham, University Park, Nottingham, NG7 2RD, UK.
[2]Centro Singular de Investigación en Química Biolóxica e Materiais Moleculares (CIQUS), Universidade de Santiago de Compostela, 15782 Santiago de Compostela, Spain.
[3]Institute of Process Research and Development, School of Chemistry, University of Leeds, Leeds, LS2 9JT, UK.
[4]Nanoscale & Microscale Research Centre, University of Nottingham, University Park, Nottingham, NG7 2RD, UK.
E-mail: andrei.khlobystov@nottingham.ac.uk

Abstract

We assemble multi-functional nanoreactors using hollow graphitised carbon nanofibers (GNFs) combined with nanocatalysts (Pd or Pt) and magnetic nanoparticles. The latter are introduced in a form carbon-coated cobalt nanomagnets ($Co@C_n$) adsorbed on GNF, or formed directly on GNF from ferrocene yielding carbon-coated iron nanomagnets ($Fe@C_n$). High resolution transmission electron microscopy (HRTEM) demonstrated that $Co@C_n$ and $Fe@C_n$ are attached effectively to the GNFs, and the loading of nanomagnets required for separation of the nanoreactors from the solution with an external magnetic field was determined using UV/Vis spectroscopy. Magnetically functionalised GNFs combined with palladium or platinum nanoparticles result in catalytically active magnetically separable nanoreactors. Applied to the reduction of nitrobenzene the multi-functional nanoreactors demonstrate high activity and excellent durability, whilst their magnetic recovery enables significant improvement in the re-use of the nanocatalyst over five reaction cycles (catalyst loss < 0.5% by wt.) as compared to the catalyst recovery by filtration (>10% catalyst loss by wt.).

1. Introduction

Carbon nanotubes are mechanically robust, thermally and chemically stable cylinders of sp^2-carbon that can be used to immobilise both molecules and nanoparticles which efficiently adsorb onto the nanotube walls and/or are encapsulated within the internal cavity of the nanotube via non-covalent interactions such as van der Waals forces.[1-8] Once the catalyst is immobilised in the hollow structure, catalytic chemical reactions which occur within the accessible nanoscale space of the nanoreactor interior can benefit from enhanced rates of reactions and selectivity.[9-27]

Specifically, Metal NPs supported in GNFs catatalysts have recently been used for a variety of different reactions, including PtNPs in C-C cross coupling reactions,[21] IrNPs in hydrosilylations,[13,18,22] and CuNPs in click chemistry.[23] In a recent study, we demonstrated that RuNPs confined in GNFs results in dramatic changes to reactions with the highest observed activity and selectivity in single and competitive hydrogenations of norbornene and benzonorbornadiene compared to unconfined RuNPs supported on single-walled carbon nanotubes (SWNT) and commercial carbon black.[24] PtNPs confined within GNF were also investigated in the oxygen reduction reaction (ORR) by Gimenez-Lopez et al. and incredible electrochemical stability was observed over 5000 cycles of ORR, with the PtNPs stabilised by the step edges significantly more strongly than commercial PtNPs on carbon black.[25] In additon to NP based catalyts, Lebedeva et al. synthesized fullerene containing and fullerene free Pd(II)Salen metal complexes and encapsulated both species on the step edges of the intenal GNF surface to form catalysts which displayed significantly higher activity and selectivity in several Heck reactions compared to the reactions in solution.[19]

Therefore, carbon nanotubes are of great interest for use as nanoreactors in a variety of different catalytic chemical reactions as they not only template the formation of catalytically active metallic nanoparticles but also influence the subsequent pathway of reactions.[11,14-27] However,
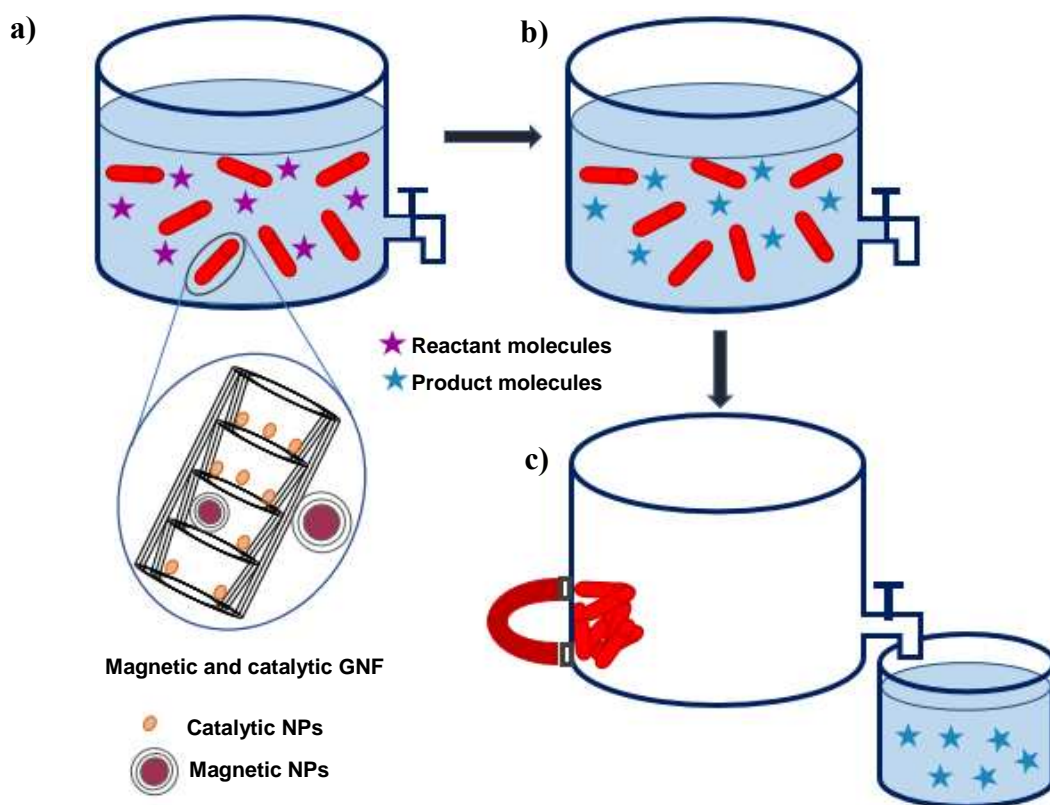
despite the fact that carbon nanotubes are excellent support materials for heterogenous catalyst systems, the inherent properties of carbon nanotubes, including their low density and hydrophobisity, makes their separation from the reaction solution using conventional separation techniques, such as filration and centrifugation challenging, meaning that currently expensive equipment and secondary processes are required.[28-30] In order to minimise the costs and technical challenges in conventional catalyst separation and facilitate the recycling of precious metal catalysts, intense research efforts have been focused on the development of magnetic supported metal nanoparticle catalysts which could be controlled by an applied magnetic field.[31-36] This approach enables the selective separation of magnetic material supporting catalysts from the reaction mixture containing the products (non-magnetic species) by application of a magnetic field.

Ferromagnetic metal nanoparticles including Fe and Co combine high catalytic activity with a non-zero magnetic moment at room temperature due to unpaired electrons, which can be useful for many catalytic reactions.[34-35] However, as these magnetic metal nanoparticles are not stable in air and easily react with acid media, resulting in a change or loss of their magnetisation, their use in preparative catalysis has been limited.[29] Therefore, an alternative route is to combine a fully protected magnetic nanoparticle component, coated with an appropriate inert material such as silica, polymers or carbon, with another, non-magnetic but catalytically active metal nanoparticle component to perform the catalysis on a suitable support material.[37-40]

Preparation of carbon-coated magnetic nanoparticles has recently received increasing attention as carbon nanomaterials have been proven to be both chemically and thermally more stable and robust than silica or polymer coatings.[41] These materials consist of magnetic nanoparticles, providing a magnetic core, and a graphene-like outer shell which ensures that the magnetic material is completely coated and protected against oxidation and erosion by strong acids or bases, allowing their use under harsh reaction conditions. A number of methods have been

3

applied to prepare carbon-coated magnetic nanoparticles, especially in the metallic phase which have higher magnetic moments compared to metal oxides, using chemical vapour deposition and the sequential spraying and controlled pyrolysis of carbon sources at elevated temperatures.[37,42-43] Recently Grass et al. developed a method to synthesise carbon-coated Co nanomagnets (Co@C$_n$) using reducing flame spray pyrolysis under an inert atmosphere.[37] This method allowed the production of nearly spherical magnetic particles with an onion-like sp^2-carbon coating with a thickness of 2-3 nm and a mean particle diameter of about 4-100 nm. It was subsequently demonstrated that it is possible to modify the carbon coating using both covalent and non-covalent functionalisation and this has been exploited to attach catalytic nanoparticles to the surface of the nanomagnets, creating magnetically recoverable heterogeneous catalysts for a variety of catalytic applications.[44-49] On the other hand, Wittmann et al. demonstrated the preparation of a palladium complex non-covalently attached to Co@C$_n$ based on strong π-π stacking interactions between pyrene units and the outermost graphene layer enabling efficient catalyst recovery.[45] Furthermore, the graphene-like outermost shell of carbon coated magnetic nanoparticles is very similar to the surface of carbon nanotubes which enables combination of the two materials via adsorption of the nanoparticles onto the exterior sidewalls or into the internal channel of the nanotubes driven by van der Waals forces.[46] The combination of catalytic carbon nanoreactors with magnetic Co@C$_n$ nanoparticles using non-covalent interactions (van der Waals forces) could potentially allow the separation of the carbon nanoreactors from reaction mixtures in a fast, easy and efficient way by simply applying a magnetic field. In this study, this idea of creating magnetically separable carbon nanoreactors which contain active metal nanoparticle catalysts confined in their channels is explored, and both the catalytic activity and the magnetically induced separation of the resultant hybrid materials are investigated.

Graphitised carbon nanofibers (GNF) were chosen as the carbon nanoreactor support as they, unlike carbon nanotubes, have negligible residual metal content making analysis of the metal nanoparticle-nanocarbon hybrids easier to quantify.[50] Furthermore, GNF have differently structured internal and external surfaces and wide, continuous internal channels, with an average internal diameter of ~50 nm. Finally, unlike carbon nanotubes, the internal surface has a succession of step edges which can act as anchoring points for guest species making GNF a highly effective nanoreactor for immobilisation of catalytic nanoparticles and to perform catalytic reactions at the nanoscale.[7, 18-19, 24-25] With this aim, we developed two different procedures for forming magnetically recyclable GNF based carbon nanoreactors: (1) in situ formation of $Fe@C_n$ inside the GNF channels, and (2) attachment of commercially available $Co@C_n$ to GNF through non-covalent interactions. In addition, we explored two different methodologies to combine the formation step of the catalytically active palladium or platinum nanoparticles with the magnetic functionalisation step. As a result, catalytically active and magnetically separable hybrid materials were successfully designed and synthesised, and their activities in the reaction of nitrobenzene reduction were tested and compared.

a)

b)

★ Reactant molecules
★ Product molecules

c)

Magnetic and catalytic GNF

◉ Catalytic NPs
◉ Magnetic NPs

Scheme 1. A schematic illustration of the recovery of catalytic GNF nanoreactors by magnetic separation from a liquid solution after a chemical reaction.

2. Results and discussions

2.1. Designing and preparing magnetically recyclable GNF based carbon nanoreactors

An experimental method was developed to make carbon-coated Fe nanoparticles directly in the GNF, ($Fe@C_n$)/GNF. In this method (Figure 1a), ferrocene was inserted from the vapour phase into GNF at 350 °C in vacuum and subsequently heated to 500 °C to decompose the ferrocene into Fe nanoparticles (NPs) coated in graphitic shells ($Fe@C_n$) which deposit on the walls of the GNF (N.B. source of carbon is cyclopendienyl ligand of ferrocene) **(Experimental section)**. High resolution transmission electron microscopy (HRTEM) imaging confirmed the presence of FeNPs coated by a graphitic shell in which the carbon interplanar distance was measured to be 0.34 nm, which is comparable to that of the interlayer spacing in graphite **(Figure 1b-1d)**. The $Fe@C_n$ nanoparticles have an average diameter of 23.9 ± 14.9 nm **(Figure 1e)** with a carbon

6

shell tickness of 5.84 ± 2.49 nm (corresponding 17 ± 7 graphene-like carbon layers), and are adsorbed principally to the stepedges of the sidewalls within the cavity of the GNF (>60 %), with the remaining Fe@C$_n$ absorbed on the outer surface of the GNF. This could be a results of the step edges providing better adsorption sites for individual ferrocene molecules during the decomposition process. Thus, as the iron-contaning material is already inside the channel, upon rapid thermal decomposition the resultant carbon-coated Fe nanomagnets are formed primarily inside the GNF channel. In addition, the concave surface of GNF interior is likely to assisst nucleation of Fe@C$_n$. Powder X-ray diffraction (XRD) revealed the presence of a metallic Fe phase which is in good agreement with the diffraction pattern of α-FeNPs reported previously **(Figure 1f)**.[52] The Fe loading (wt.%) in the (Fe@C$_n$)/GNF was quantified using TGA by heating in air up to 1000 °C at a rate of 10 °C per minute **(Figure 1g)**. TGA showed that the presence of Fe in (Fe@C$_n$)/GNF led to a significant decrease in the oxidation temperature of the GNF from ~700 °C to ~500 °C. At ~850 °C a small weight gain, presumably due to oxidation of the Fe, was observed. Therefore, the residual Fe content (wt.%) was recorded as the average mass between 820-850 °C, and was observed to be 8.5 ± 0.6 wt.%, **(Figure 1g)**.
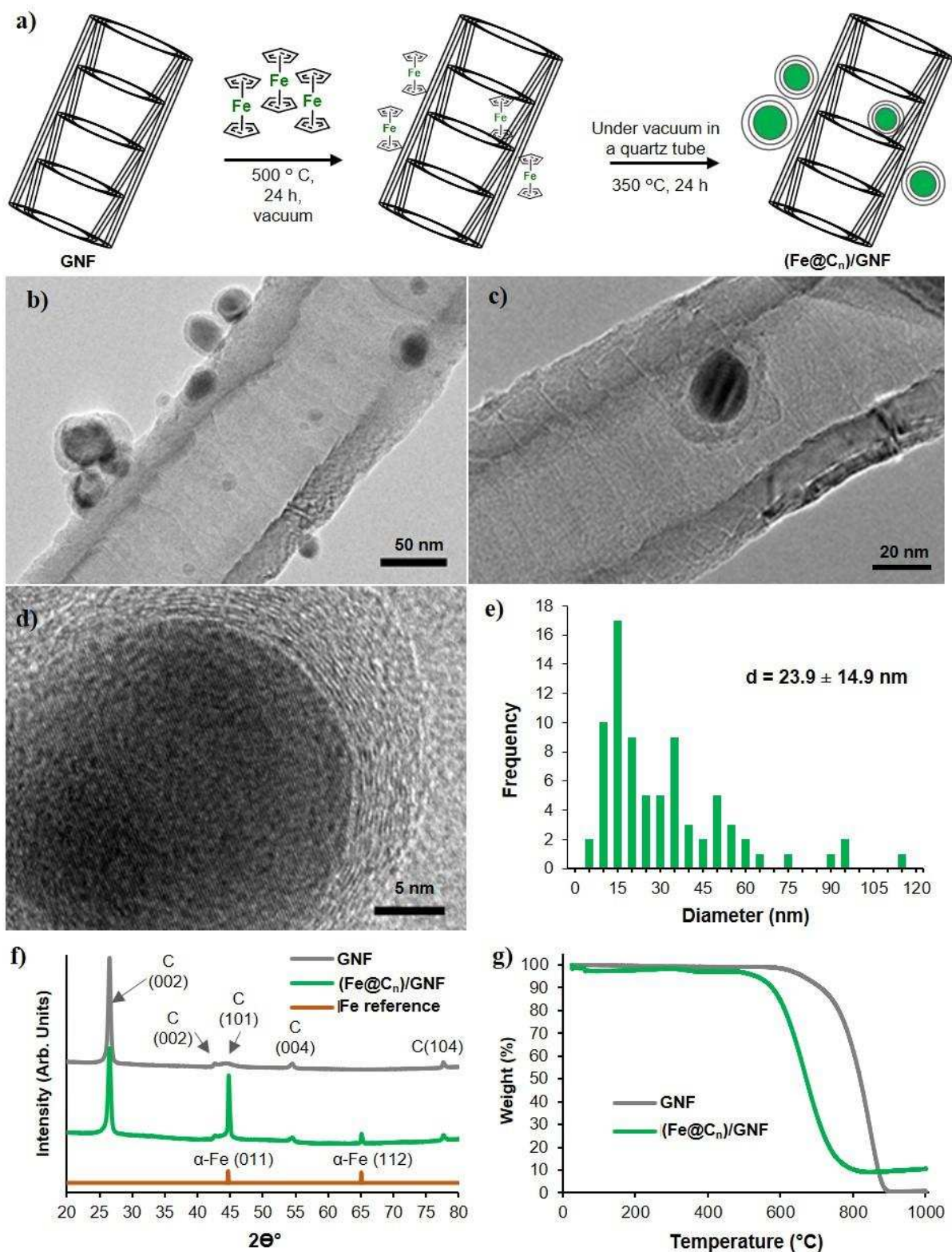
Figure 1. (a) Schematic illustration of the experimental procedure for synthesis of carbon coated FeNPs attached to GNF ((Fe@C$_n$)/GNF), (b-c) HRTEM images of (Fe@C$_n$)/GNF where the graphene layers can be seen in the close-up of the particle, (d) particle size distribution of Fe@C$_n$ (the size of Fe and graphitic shell were measured together using more than 80 particles) (f) Powder XRD patterns and (g)TGA measurements of (Fe@C$_n$)/GNF in air at a heating rate of 10 °C/min.

To test the implications of the magnetic confinement on the development of magnetically recyclable GNF based carbon nanoreactors, commercially available magnetic $Co@C_n$ were also attached to individual GNFs using non-covalent interactions. As carbon nanostructures are known to be attracted to each other by strong van der Waal forces (0.5 eV/Mm), a good solvent was required to obtain well-dispersed and separated GNFs[51] to ensure good mixing with $Co@C_n$. Therefore, GNFs were initially dispersed using ultrasonic treatment in hexane. $Co@C_n$ were also dispersed using the same method, and then added to the hexane/GNF dispersion very slowly whilst being continuously treated with ultrasonic waves to create a material in which the $Co@C_n$ nanoparticles are adsorbed on the GNF, $(Co@C_n)$/GNF (**Figure 2** and **Experimental section**). The minimum loading of $Co@C_n$ required for complete separation of the composite material from solution was evaluated by changing the amount of magnetic $Co@C_n$ in the $(Co@C_n)$/GNF material and exposing each sample, suspended in hexane, to an external magnet and evaluating the resulting solution by eye. $(Co@C_n)$/GNF was prepared in 1, 5 and 10 % by wt. of $Co@C_n$ on GNF, and the resultant $(Co@C_n)$/GNF materials were separated from the solvent by applying an external magnetic field using a commonly available neodymium magnet with a magnetic strength of ~0. 1 Tesla (T). Complete separation for $(Co@C_n)$/GNF containing 10 % of $Co@C_n$ was achieved (Experimental section 4.2). Lower $Co@C_n$ loadings, however, resulted in incomplete separation compromising the recovery of all the catalyst material that is strictly required when pursuing recyclable catalytic materials **(Figure S1)**. The $(Co@C_n)$/GNF sample with 10 % by wt. loading was then characterised by HRTEM, thermogravimetric analysis (TGA) and powder XRD. HRTEM confirmed the presence of very-well distributed $Co@C_n$ on both the outer and interior surfaces of the GNF with an average diameter of $Co@C_n$ 29.7 ± 22.8 nm **(Figure 2)**, with a carbon shell tickness of 2.87 ± 1.19 nm (corresponding 7 ± 4 graphene-like carbon layers).
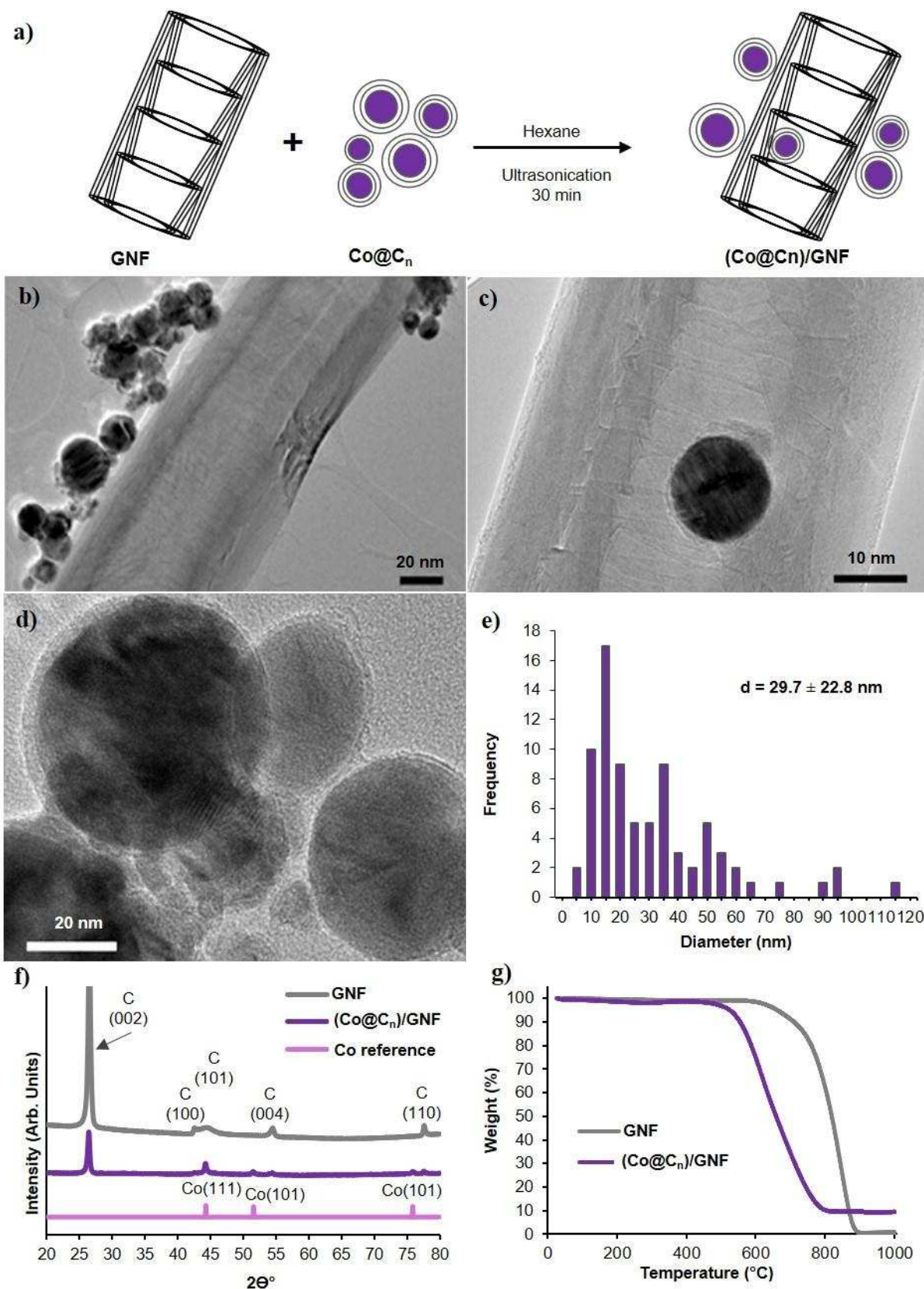
Figure 2. a) HRTEM image of the commercial graphene like carbon covered cobalt nanomagnets (Co@C$_n$) where the graphene layers can be seen in the close-up of the particle, b) particle size distribution of Co@C$_n$ (the combined diameter of the Co NP and graphitic shell were measured for more than 80 particles). HRTEM images of Co@C$_n$/GNF material showing the Co$_n$@C non-covalently attached to the inner (c) and outer (d) GNF sidewalls.

In contrast, to the Fe@C_n/GNF system, the majority of the Co@C_n nanomagnets are adhered to the GNF outer surface (>90 %), presumably due to the more readily accessible and aromatic character of the outer sureface of GNF resulting in a higher affinity for Co@C_n than the corrugated, step-edge containing internal channels. The smooth graphitic shell of the Co@C_n is likely to be engaged in π-π stacking interactions with the smooth exterior of GNF and thus results in stronger van der Waals forces between the Co@C_n and the GNF outer surface. There will also undoubtly be an energetic barrier to diffusion of the larger Co_n@C_n down the internal channel of the GNF as a result of their similar sizes. The composition of the (Co@C_n)/GNF was determined by powder XRD showing the presence of a metallic cobalt phase which is in good agreement with the reference fcc-Co metal powder XRD pattern (**Figure 2f**).[52] Similar to (Fe@C_n)/GNF, TGA was used to identify the degree of magnetic metal loading in (Co@C_n)/GNF after heating in air up to 1000 °C at a rate of 10 °C per minute (**Figure 2g**). TGA studies of (Co@C_n)/GNF showed that the presence of Co led to a significant decrease in the oxidation temperature of the GNF from ˜ 700 °C to 500 °C. The weight gain observed between ˜800 °C and 1000 °C due to oxidation of the residual Co after the carbon shells have been removed was negligible, however, to ensure this was accounted for the residual weight was recorded as an average value between 800-850 °C and revealed the (Co@C_n)/GNF material to be 8.5 ± 0.5 % by wt. which is comparable to the metal loading observed within (Fe@C_n)/GNF.

2.1.1. Evaluating the efficiency of the magnetic separation of (Fe@C_n)/GNF and (Co@C_n)/GNF

Separation of the resultant functionalised GNF composite suspensions from the solvent was achieved by placing a magnet (0.1 T) on the external wall of the sample tube for a short period of time (90 s) (**Figure 3a**). The effect of varying the extent of loading of both Fe@C_n and Co@C_n on the separation of the GNFs was evaluated using an ultraviolet–visible (UV-Vis)

spectroscopy in which (Fe@C_n)/GNF and (Co@C_n)/GNF samples were suspended separately in hexane by stirring, and then exposed to an external magnet for different lengths of time **(Experimental section)**. UV-Vis spectroscopy was used to evaluate the concentration of Fe@C_n/GNF and Co@C_n/GNF that remained suspended in the hexane after application of the magnet. We used the intensity of optical density measured by UV-Vis spectroscopy to determine the concentration of GNF-magnetic material composite remaining as a suspension after magnetic separation at the visible wavelength range, 350-700 nm, assuming that the optical density is directly proportional to the concentration of GNF in solution, in accordance with the Beer-Lambert law.[53-54] UV-Vis spectroscopy measurements for the separation of each material follow a linear trend over time at a single wavelength (500 nm) **(Figure 7c)**. The optical density is observed to decrease over time upon application of the magnetic field for each material demonstrating excellent separation rates for both materials after exposure to the magnetic field for ~ 90 s **(Figure 3)**. However, (Co@C_n)/GNF is observed to reach lower optical densities faster than (Fe@C_n)/GNF, which indicates that (Co@C_n)/GNF is separated from hexane more rapidly.
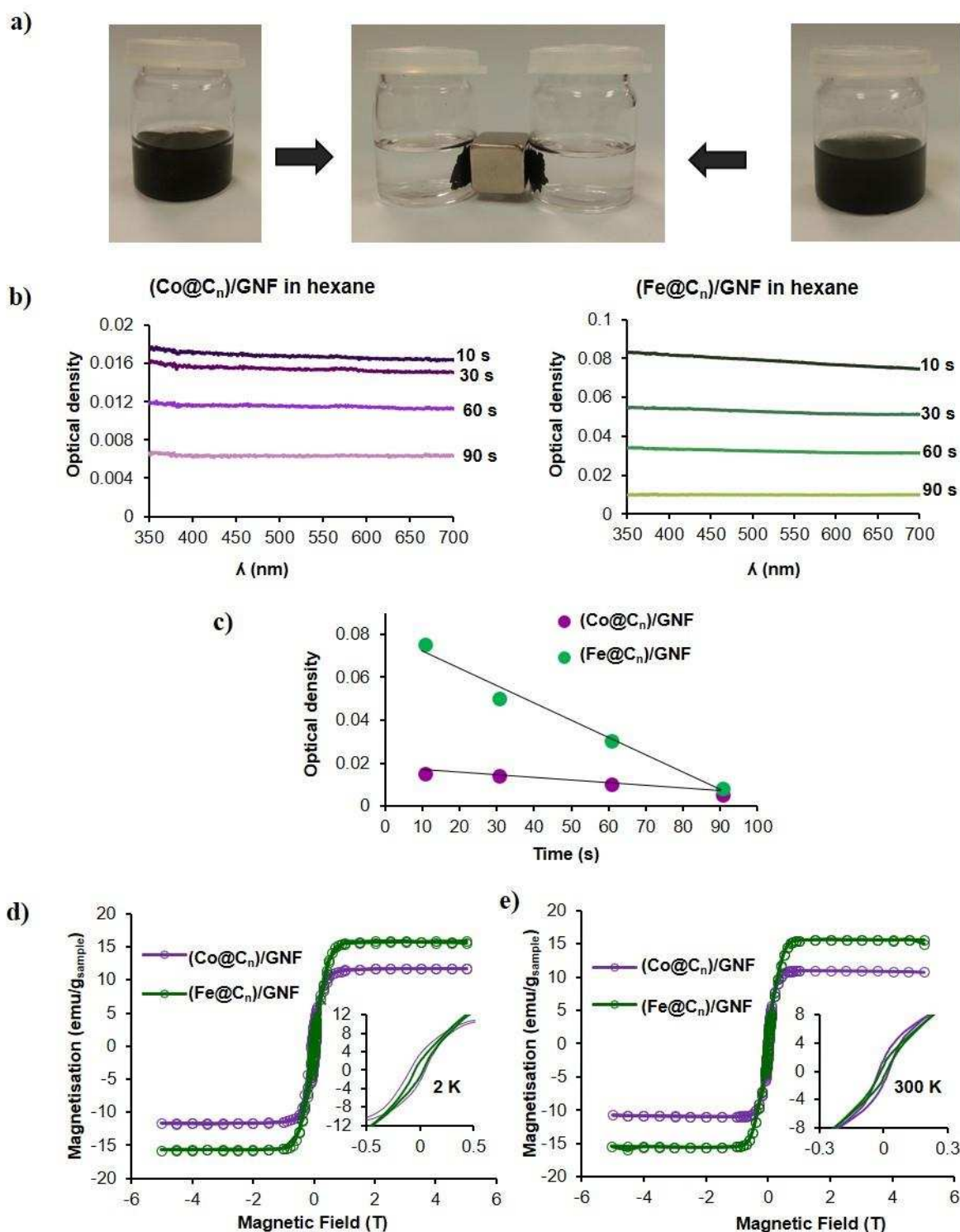
Figure 3. a) Suspensions of (Co@C$_n$)/GNF (left) and (Fe@C$_n$)/GNF (right) after applying a magnetic field for 90 s. b) UV-Vis measurements for the solutions of Co@C$_n$/GNF (left) and (Fe@C$_n$)/GNF (right) after magnetic separation at various times. c) Plot of optical density at 500 nm of the solutions from (Co@C$_n$)/GNF and (Fe@C$_n$)/GNF separations in hexane versus the length of time that the magnetic field (0.1 T) was applied for. d) Magnetic hysteresis loops for (Co@C$_n$)/GNF and (Fe@C$_n$)/GNF recorded at 300 K (inset: expanded region at low magnetic fields between -0.5 and 0.5 T).

In order to explain this difference on separation rates, we have studied the magnetic properties of (Co@C$_n$)/GNF and (Fe@C$_n$)/GNF **(Experimental section)**. The magnetic response of both systems under an applied magnetic field displayed hysteresis loops **(Figure 3d-3e)** and exhibited the magnetic parameters summarised in Table S1 tipical for ferromagnetic systems. While at 5 T (Fe@C$_n$)/GNF reaches higher magnetic saturation values than (Co@C$_n$)/GNF at both 2 K and 300 K, at low magnetic fields (< 0.1 T) the magnetisation values observed for (Co@C$_n$)/GNF are slightly higher than that of the Fe analogue. These observations are also in agreement with the thermal variation measurements of the magnetisation performed for both materials at 0.1 T that showed higher magnetisation values for (Co@C$_n$)/GNF than that of (Fe@C$_n$)/GNF in the temperature range 2-300 K **(Figure S2)**. These results are consistent with our UV-vis measurements for which we observed a better separation with (Co@C$_n$)/GNF in comparison to (Fe@C$_n$)/GNF when a small magnetic field (< 0.1 T) was applied for the separation at room temperature.

2.2. Catalytic chemical reactions within magnetically recoverable carbon nanoreactors

2.2.1. Preparing and testing catalytic carbon nanoreactors

After successful demonstration of the magnetic separation of (Co@C$_n$)/GNF and (Fe@C$_n$)/GNF nanoreactors, the next step was to introduce catalytically active metal nanoparticles within the GNF nanoreactors in order to utilise these materials in a suitable catalytic reaction. The methods selected here must be compatible with the proposed magnetically recyclable GNF based carbon nanoreactors. To illustrate the catalytic activity of our magnetically separable hybrid materials, the reduction of nitrobenzene was chosen in this work as a model reaction, as it is very important reaction both in industry and academia, with aniline used as a key precursor in the synthesis of chemicals, dyes and pharmaceuticals.[56]

Palladium (PdNPs) and platinum nanoparticles (PtNPs) were selected as they have been demonstrated as highly active catalysts for the solution phase reduction of nitrocompounds previously.[54-62] In addition, they are both paramagnetic metals, so no competing magnetic effects are expected in the final composite materials. The formation of Pd and Pt nanoparticles supported by the GNF nanoreactor (MNPs@GNF; MNPs stands for metal nanoparticles where M = Pd or Pt) was initially investigated in the absence of the magnetic nanoparticles to optimsie formation conditions of PtNP and PdNP in GNFs using suitable metal procrursors, (Experimental section for details), and then tested in the reduction of nitrobenzene using a high pressure H_2 glass vessel (**Scheme S1**). PdNPs@GNF-1 was produced by the thermal decompostion of Pd(acac)$_2$ to form Pd nanoparticles inside the GNF using vaccum filling conditions. The formation of PdNPs was confirmed by HRTEM revealing an average particle size of 10.79 ± 3.86 nm (**Experimental section and Figure S3a-b**) and the PdNPs to be located solely at the step edges in the GNF internal channel, while PdNPs@GNF-2 synthesied in solution from Pd$_2$dba$_3$[66] in GNFs (**Experimental section**) resulted in the formation of very small and well distributed PdNPs, observed mostly inside the GNF attached to the step-edges, as revealed by HRTEM, with an average PdNP diameter of 2.26 ± 0.56 nm (**Figure 4b and 4d**).
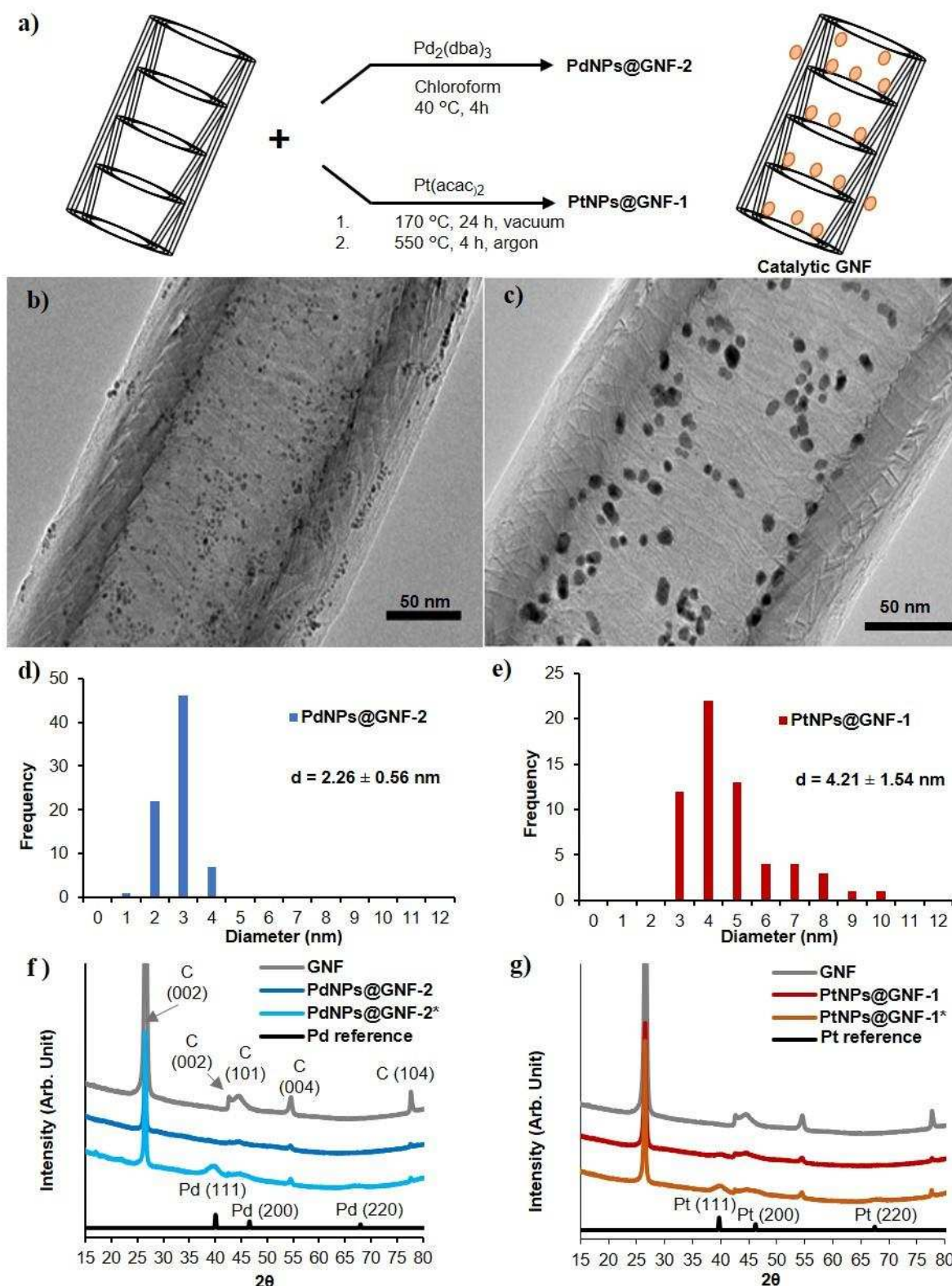
Figure 4. (a) Schematic and (b-c) representative HRTEM images of (b), PdNPs@GNF-2, and (c), PtNPs@GNF-1, (0.5 % by wt. metal in both cases), and (d) and (e) the histograms showing the size distribution of the PdNPs and PtNPs in their respectively composites. Powder XRD patterns of (f), PdNPs@GNF-2, and (g), PtNPs@GNF-1. Diffractograms for Pd and Ptreferences and GNF (annealed at 450 °C for 1 (h)) are shown for comparison. All * composites show 15 % by wt. loading of Pt or Pd respectively for comparison.

16

The powder XRD for PdNPs@GNF-1 showed the presence of metallic Pd **(Figure S4)** but PdNPs@GNF-2 did not exhibit clear Pd diffraction patterns due to very small size of the PdNP in this material.[67] Therefore, we synthesised a control material, PdNPs@GNF-2*, with a higher metal loading (15 % Pd by wt.) using the same procedure as for PdNPs@GNF-2 and observed distinctive Pd diffraction patterns by XRD confirming decomposition of the starting material to metallic palladium **(Figure 4f)**.

PtNPs@GNF-1 and PtNPs@GNF-2 were produced using the $Pt(acac)_2$ and $Pt(dba)_3$[68], using similar experimental proceduresto those for PdNPs@GNF-1 and PdNPs@GNF-2, respectively **(Experimental section)**. HRTEM imaging of PtNPs@GNF-1 showed Pt nanoparticles distributed along the step-edges of the nanoreactor with an average particle size of 4.21 ± 1.54 nm (Figure 4c and 4e), and for PtNPs@GNF-2 much smaller nanoparticles with an average size of 1.55 ± 0.48 nm located mostly in the interior of the nanoreactor **(Figure S3g-h)**. The powder XRD did not exhibit clear diffraction peaks for metallic platinum in both PtNPs@GNF-1 and PtNPs@GNF-2 due to the small size of Pt nanoparticles **(Figure S4)**. We repeated the synthesis of these material using a higher metal loading (15% Pt by weight) resulting in bigger nanoparticles, allowing clear diffraction patterns of metallic platinum to confirm the presence of metallic PtNP for both materials **(Figure S4)**. [69]

The reduction of nitrobenzene was then carried out in the presence of all obtained catalysts using high pressure glass equipment and molecular H_2, and quantified by ^{1}H NMR **(Experimental section)**. The lower catalytic activity of PdNP@GNF-1 compared to PdNPs@GNF-2 is attributed to the larger nanoparticle size, and thus lower catalytic surface area of the PdNPs in PdNPs@GNF-1. In contrast, no reactivity was observed for the smaller PtNPs in PtNPs@GNF-2 compared to the larger PtNPs in PtNPs@GNF-1, which were observed to be surprisingly active **(Table 1)**. The reason for the lack of reactivity for the small

PtNPs in PtNPs@GNF-2 requires further investigation but we propose that such small nanoparticles could be quite amorphous and therefore have poorly defined sites for catalysis, or may contain some residual dba ligand blocking the surface. The lack of crystallographic planes observed in XRD and HRTEM supports the former argument. Due to the lack of reactivity of PdNPs@GNF-1 and PtNPs@GNF-2, we did not further investigate these materials in the reduction of nitrobenzene. Therefore, PdNPs@GNF-2 and PtNPs@GNF-1, which both showed significant activity and high aniline selectivity (compared to n-phenylhydroxylamine), were chosen for the design of catalytcially active magnetically separable nanoreactors.

The BET surface area of PdNPs@GNF-2 and PtNPs@GNF-1 was investigated to enable the number of active sites for each catalyst to be approximated **(Table S2 and Figure S5)**. As we reported in our previous study[24], empty GNF have a surface area of 12 m^2/g and contain mesoporous (2-50 nm) and some macroporous (> 50 nm) pores in the carbon structure which is consistent with the size of the step edges (height = 3-5 nm) and the inner channel of the GNF (diameter = 10-100 nm). After adding Pd or Pt nanoparticles to the GNF, BET surface area of the material increased in both cases, ~16.0 m^2 g^{-1} for PdNPs@GNF-2 and ~15.7 m^2 g^{-1} for PtNPs@GNF-1 attributed to the precence of metal nanoparticles in the GNF. Therefore, by substracting surface area of GNF from MNP@GNF, surface areas of PdNPs and PtNPs are estimated to be 4.0 m^2 g^{-1} and 3.7 m^2 g^{-1} respectively.

Table 1. Reaction data for the reduction of nitrobenzene using PdNP@GNF and PtNP@GNF catalytic nanoreactors using a high pressure H_2 glass reactor.
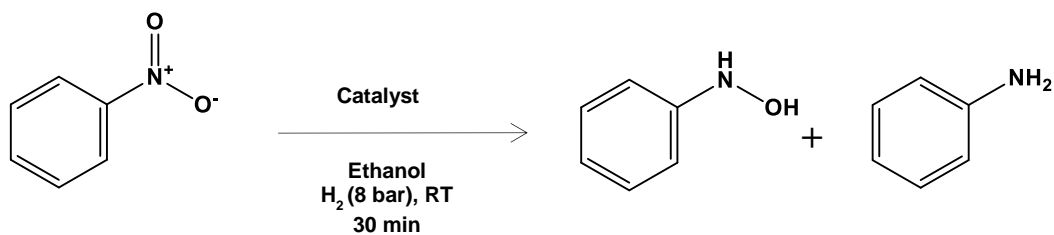
Catalyst	Time	Conversion of Ph-NO$_2$ (%)	Selectivity (%)	
			Ph-NHOH	Ph-NH$_2$
-	24 h	0	0	0
GNF[a]	24 h	0	0	0
PdNPs@GNF-1	30 min	3.5	71	29
PdNPs@GNF-2	30 min	77	15	85
PdNPs@GNF-2	50 min	100	0	100
PtNPs@GNF-1	30 min	24	36	64
PtNPs@GNF-1	200 min	100	0	100
PtNPs@GNF-2	30 min	0	0	0
PtNPs@GNF-2[b]	24 h	0	0	0

Reaction conditions: Nitrobenzene (0.78 mmol), ethanol (0.5 mL), catalyst (0.00047 mmol of metal), H_2 (8 bar), room temperature. All reactions were performed in duplicate and nitrobenzene conversion was determined by ^{1}H NMR with an error of ± 2 %. [a]GNF were annealed at 450 °C for 1 hour prior to use. [b]PtNPs@GNF-2 was annealed under H_2 flow for 5 h at 150 °C prior to the reaction to get rid of any impurities on the surface of Pt which can cause deactivation of the catalyst.

2.3. Magnetically recoverable catalytic nanoreactors

Two different methodologies were explored for fabrication of magnetically recoverable catalytically active carbon nanoreactors.
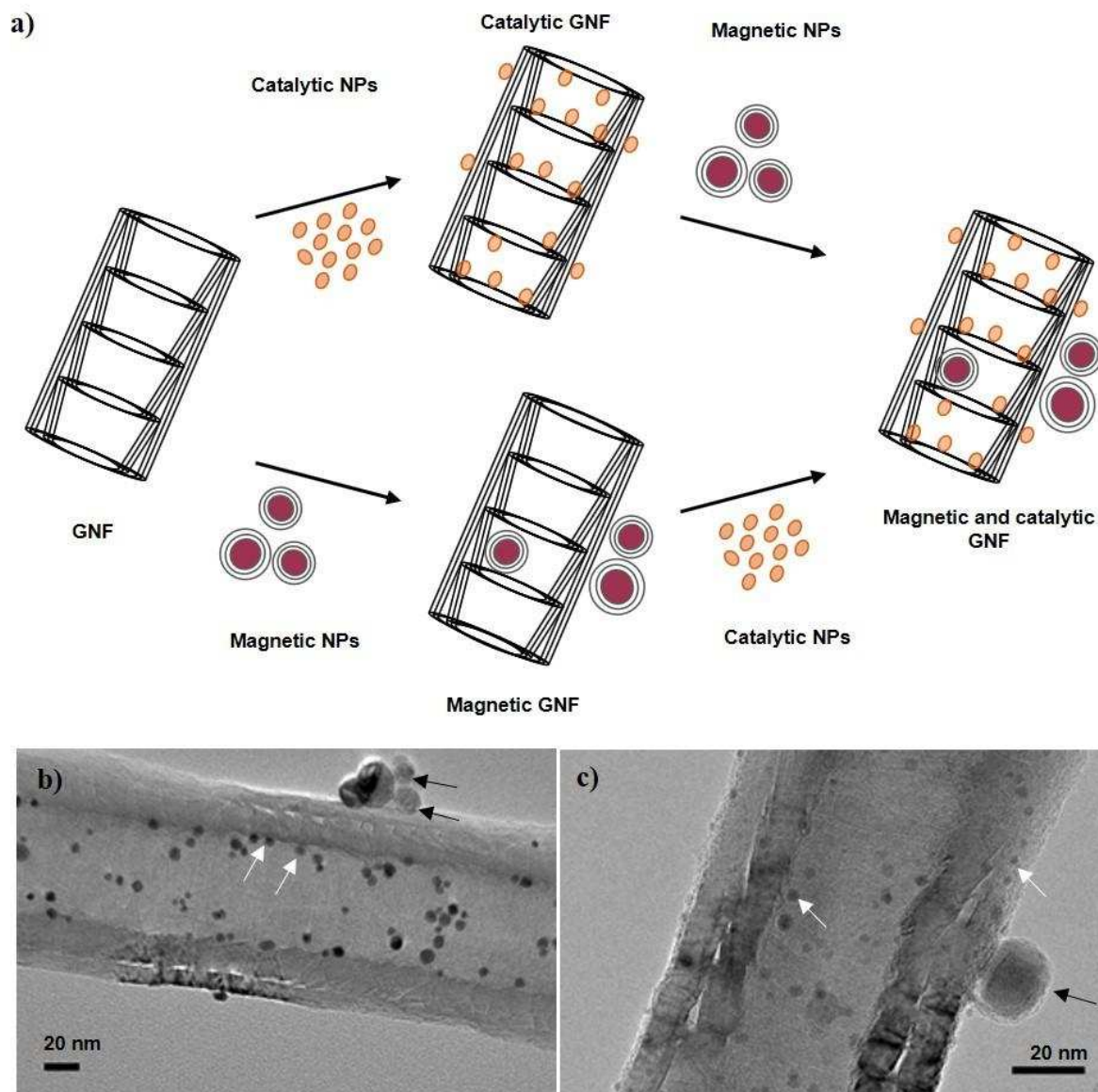
Figure 5. (a) Schematic showing the two different approaches taken to form magnetic catalytically active carbon nanoreactors. TEM images of (b), $PtNPs@((Co@C_n)/GNF)$ and (c), $PtNPs@((Fe@C_n)/GNF)$; white and black arrows indicate positions of catalytic and magnetic nanoparticles respectively.

In the first approach, catalytic PdNPs or PtNPs were encapsulated within GNF using the solution method and gas phase filling method respectively (as desctibed for PdNPs@GNF-2 and PtNPs@GNF-1 above) and then subsequently combined with $Co@C_n$ in hexane using the

ultrasound conditions previously optimised **(Experimental sections)**, thus yielding PdNPs@((Co@C$_n$)/GNF) and PtNPs@((Co@C$_n$)/GNF), with HRTEM analysis confirming the successful adsorbtion of Co@C$_n$ on ther outer surface of the PdNPs@GNF and PtNPs@GNF nanoreactors **(Figure S7)**. To fabricate catalytic magnetic nanoreactor from Fe@C$_n$, the magnetic component was produced initially to give (Fe@C$_n$)/GNF and then the catalytic PdNPs or PtNPs were encapsulated within (Fe@C$_n$)/GNF using solution or gas phase filling methods, respectively **(Experimental section)**. HRTEM images of PdNPs@((Fe@C$_n$)/GNF) and PtNPs@((Fe@C$_n$)/GNF) confirm successful formation of the two MNPs@(Fe@C$_n$)/GNF materials **(Figure S7)**.

2.3.1. Catalytic chemical reactions within magnetically recoverable MNPs@((Fe@C$_n$)/GNF) and MNPs@((Co@C$_n$)/GNF) catalysts

Performance of the magnetic catalytically active nanoreactors was tested in the nitrobenzene reduction reaction **(Table 2)**. Both PdNPs@((Co@C$_n$)/GNF) and PdNPs@((Fe@C$_n$)/GNF) performed very similarly, exhibiting nitrobenzene TOFs of 69.5 and 69.1, respectively. This is also very similar to the catalytic performance of the PdNPs@GNF-2 in the absence of the magnetic nanomaterials (c.f. TOF 69.1). PtNPs@((Co@C$_n$)/GNF) and PtNPs@((Fe@C$_n$)/GNF) also exhibited similar reactivity to each other (TOFs of 24.1 and 23.2, respectively) and to the unmodified PtNPs@GNF-1 catalyst (c.f. TOF of 25.2). All these experiments demonstrate that (Co@C$_n$)/GNF and (Fe@C$_n$)/GNF do not adversely affect the activity of the catalytic metal or product selectivity in nanoreactors.

Table 2. Reaction data for the reduction of nitrobenzene using (Co@C_n)/GNF, PdNPs@((Co@C_n)/GNF) and PtNPs@((Co@C_n)/GNF), (Fe@C_n)/GNF, and PdNPs@((Fe@C_n)/GNF) and PtNPs@((Fe@C_n)/GNF) catalysts using a high pressure H_2 glass reactor.

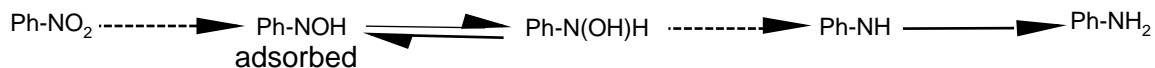| Catalys	Conversion of Ph-NO$_2$	Selectivity (%)	
	(%) / TOF (min^{-1})	Ph-NHOH	Ph-NH$_2$
PdNPs@GNF-2	77 / 72.3	15	85
PtNPs@GNF-1	24 / 25.2	36	64
(Co@C$_n$)/GNF	0	0	0
PdNPs@((Co@C$_n$)/GNF)	74 / 69.5	14	86
PtNPs@((Co@C$_n$)/GNF)	23 / 24.2	43	57
(Fe@C$_n$)/GNF	0	0	0
PdNPs@((Fe@C$_n$)/GNF)	72 / 69.1	16	84
PtNPs@((Fe@C$_n$)/GNF)	22 / 23.2	32	68

Reaction conditions: Nitrobenzene (0.08 mL, 0.78 mmol), ethanol (0.5 mL), catalyst (0.00051 mmol), H_2 (8 bar), room temperature, 30 min. All reactions were performed in duplicate and nitrobenzene conversion was determined by ^1H NMR with an error of ± 2 %. The TOFs were calculated as the ratio of the number of molecules of substrate consumed in the reaction per the number of true active catalyst sites calculated by BET measurements per minute.

Several studies have reported the reduction of nitro compounds under high pressures and temperatures in the presence of Pd and Pt catalyst supported by different materials.[56-65] Karwa et al. studied the effect of reaction temperature, hydrogen pressure and solvent on the selectivity of reduction of nitrobenzene in the presence of Pd and Pt catalysts on carbon supports and reported the formation of phenylhydroxylamine as a by-product at low temperatures, and a better selectivity for phenylhydroxylamine in the presence of Pt catalysts compared to Pd catalysts.[57] They also demonstrated that hydrogen pressures between 7-21 atm do not alter the selectivity of the reaction, however, the solvent significantly affected the selectivity for

phenylhydroxylamine, especially in solvents with higher dielectric constants such as methanol (32.7), which gave lower selectivity for aniline. This is rationalised as a result of the increased solubility and thus desorption of phenylhydroxylamine from the catalyst into the solvent preventing further hydrogenation to aniline. Takenaka et al. studied Pt/C and Pt/SiO$_2$ in the reduction of nitrobenzene at room temperature using molecular hydrogen (1 and 10 bar) and observed very high selectivity for phenylhydroxylamine (>95%).[61] These results are consistent with our data in which we observed a higher selectivity for phenylhydroxylamine in the presence of PtNPs@GNF-1 compared to PdNPs@GNF-2, while getting higher aniline selectivity overall for each catalyst. Sangeetha et al. studied Pd supported on hydrotalcite (HT), MgO and γ-Al$_2$O$_3$ between 225-300 °C and obtained the best activity in the presence of Pd/HT with a maximum turnover frequency of ~0.8 s^{-1} (48 min^{-1}).[60] Gelder et al. investigated the catalytic ability of Pd supported on different active carbon materials in the reduction of nitrobenzene using methanol and isopropyl alcohol as solvents at 50 °C and observed better catalytic activity in methanol with a turnover frequency of 0.27 s^{-1} (16.2 min^{-1}), significatly lower than to our PdNPs@GNF-2 (c.f. our TOF = 72.3 min^{-1}).[58]

The mechanism of nitrobenzene reduction is still not fully understood. However, the Haber mechanism is generally accepted in the literature and involves two different reaction routes - direct and indirect.[56-62, 67] The direct route is based on the reduction of nitrobenzene to nitrosobenzene (Ph-NO) and consecutive formation to phenylhydroxylamine (Ph-NHOH) and aniline (Ph-NH$_2$). In the light of the Haber mechanism, several research groups have proposed different additions/alterations to the reduction mechanism.[70-73] Gelder et al.[71] recently proposed a new mechanism which is contrary to the Haber process and showed that nitrosobenzene cannot be an intermediate in the formation of aniline. Our study revealed reduction of nitrobenzene to phenylhydroxylamine to form aniline which is consistent with the direct Haber process, however we did not observe nitrosobenzene or any other side products.

We therefore propose that in our nanoreactors the reaction pathway is consistent with the Gelder mechanism **(Scheme 2)**.

$$Ph\text{-}NO_2 \dashrightarrow Ph\text{-}NOH \text{ (adsorbed)} \rightleftharpoons Ph\text{-}N(OH)H \dashrightarrow Ph\text{-}NH \longrightarrow Ph\text{-}NH_2$$

Scheme 2. Proposed reaction pathways of the reduction of nitrobenzene.

2.3.2. Catalyst durability tests in the magnetic recovery process of MNPs@(Co@C$_n$)/GNF and MNPs@(Fe@C$_n$)/GNF

We investigated the reusability and durability of PdNPs@(Co@C$_n$)/GNF, PdNPs@(Fe@C$_n$)/GNF, PtNPs@(Co@C$_n$)/GNF and PtNPs@(Fe@C$_n$)/GNF in the reduction of nitrobenzene. In each case the magnetic nanoreactor catalyst was separated from the product after each run by applying a magnetic field and reused after washing with ethanol and drying in air without any other treatment and compared to the corresponding PdNPs@GNF-2 and PtNPs@GNF-1 system recovered by traditional filtration using a PTFE membrane filter and washing with ethanol **(Table S3-4 and Figure 6a-b)**. Recyclability tests showed a significant decrease in nitrobenzene conversion during the five recoveries of each catalyst, however, in each case magnetic recovery resulted in slightly lower loss of activity during the five runs compared to traditional catalyst recovery by filtration.
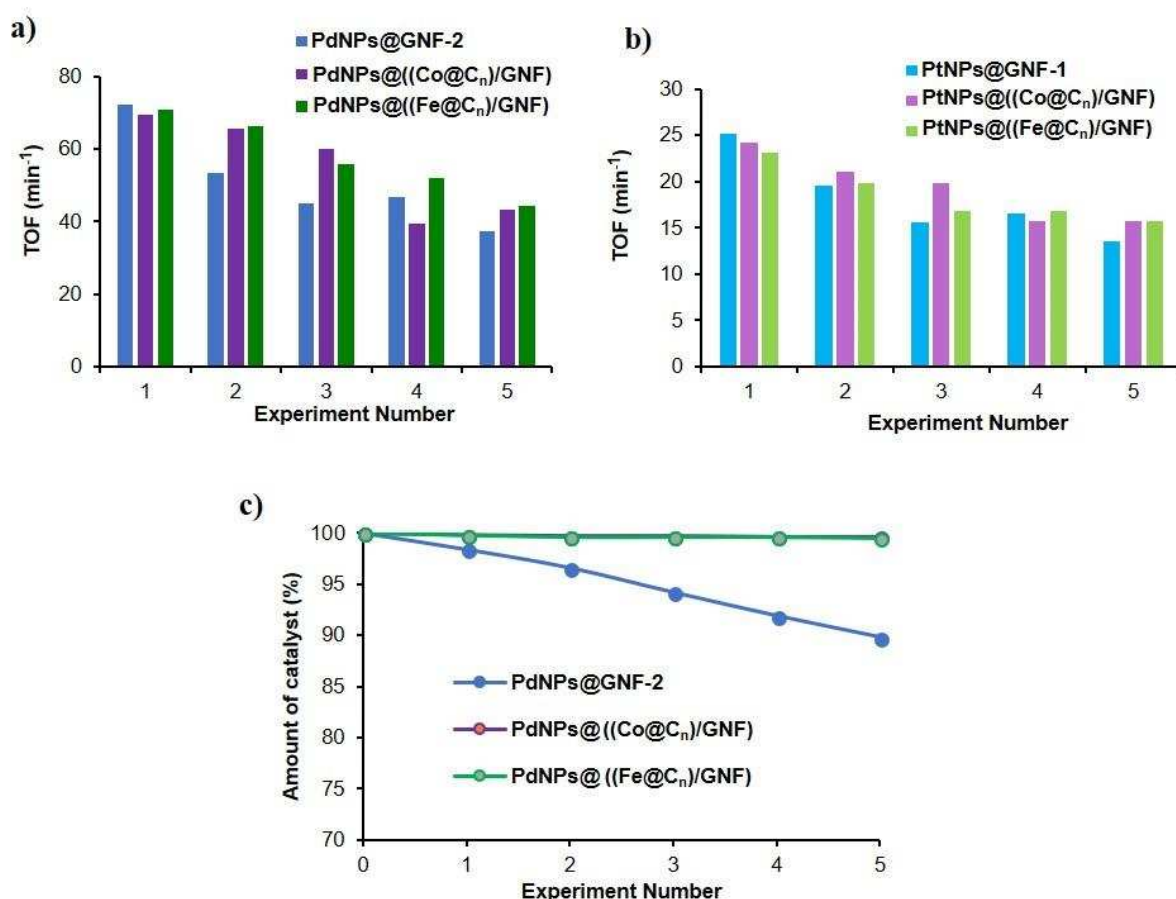
Figure 6. (a) Comparison of the catalyst TOF for nitrobenzene conversion during the five consecutive reduction reactions in which PdNPs@GNF-2 was recovered by filtration on a PTFE membrane and PdNPs@(($Fe@C_n$)/GNF) and PdNPs@(($Co@C_n$)/GNF) by magnetic separation. (b) Comparison of the catalyst TOF for nitrobenzene conversion during the five consecutive reduction reactions in which PtNPs@GNF-1 was recovered by filtration on a PTFE membrane paper and PtNPs@(($Fe@C_n$)/GNF) and PtNPs@(($Co@C_n$)/GNF) by magnetic separation. (c) Comparison of the loss of PdNPs@GNF-2 catalyts material during five consecutive nitrobenzene reduction reactions. The recovery of PdNPs@GNF-2 was achieved by filtration using a PTFE membrane, whilst PdNPs@(($Fe@C_n$)/GNF) and PdNPs@(($Co@C_n$)/GNF) were recovered by applying magnetic separation.

To further explore the reasons for decrease in catalytic activity by traditional recovery compared to magnetic recovery, the PdNP@GNF catalysts, PdNPs@GNF-2 after traditional recovery and PdNPs@(($Co@C_n$)/GNF) and PdNPs@(($Fe@C_n$)/GNF) by magnetic recovery, were weighted after each recovery step and an appreciable loss is observed, c.f. 10 % by traditional recovery as compared to <0.5 % by magnetic recovery during the five cycles (**Figure 6c**). The principle cause of catalyst loss during filtration is that some of the material it is irreversibly absorbed onto the PTFE membrane filter. The reduced activity of each catalyst

25

during the reaction, using both filtration and magnetic recovery, is most likely to be related to coarsening of the nanoparticles during the process, along with the leaching of Pd and Pt into the reaction medium. To probe whether there is a loss of catalytically active metal from the GNF by leaching, the precise metal loading of both PdNPs@GNF-2 and PtNPs@GNF-1 as synthesised and recovered after five cycles was determined by inductively coupled plasma optical emission spectrometry (ICP-OES) revealing a 3.76 % leaching of the PdNPs from GNF compared to a 3.56 % leaching of PtNPs **(Table S5)**.

These results imply that the leaching of Pd and Pt nanoparticles from the GNF is very low and therefore cannot be the reason for the reduction of the catalyst activity during the recycling. However, nanoparticle coarsening via Ostwald ripening or particle migration and coalescence, could also be occurring that would result in a decrease in active catalyst surface area, and thus a reduction of the activity of catalyst. Therefore, HRTEM imaging of the catalytic nanoreactors after five reaction cycles was performed **(Figure S8)**, showing some aggregation of the PdNPs, and excellent dispersion of the PtNPs in PdNPs@GNF-2 and PtNPs@GNF-1, respectively. Interestingly the average particle sizes after the fifth cycle measured by HRTEM of 2.4 ± 0.4 nm for the PdNPs, and 4.4 ± 1.0 nm for the PtNPs, were almost identical to the average size of the nanoparticles before the reaction. Therefore, the reduction in activity must be related to other factors, such as re-ordering of the nanoparticle structure or poisoning of the surface, with further work required to clarify this.

Conclusions

We have developed and compared several approaches for fabricating catalytically active nanoreactors, containing Pt or Pd nanoparticles confined within GNF, functionalised with carbon-coated Co or Fe nano-magnets attached to surfaces of the nanoreactors. Both, Co and Fe nano-magnets enable the facile separation of catalytic nanoreactors from the products mixtures in a fast, easy and efficient way by simply applying a magnetic field. This has

significant advantages over cumbersome and energy consuming filtration methods, traditionally used for separation of catalysts.

The catalytic performance of Pt- and PdNPs encapsulated in GNF was probed in the reduction of nitrobenzene with both materials exhibiting excellent activity and selectivity, especially PdNPs@GNF. Importantly, adsorbtion of the magnetic nanoparticles $Co@C_n$ or $Fe@C_n$ on the exterior of the catalytic nanoreactors was found to have no negative effects on the catalytic performance, while significatly reducing the loss of catalytic material over five cycles of reaction, compared to filtration.

Magnetic nanoreactors allow a combination of retention and recyclability of catalytically active metals offered by the GNF cavity, with the magnetic functionality enabling facile re-use of the catalytic material. This study lays the foundations for generation of a diverse family of magnetically separable carbon nanoreactors and gives guidance for future development of metal-catalysed reactions in magnetic carbon nanoreactors, which in the long term can be scaled-up and applied for chemical processes of industrial importance streamlining catalysis and synthesis.

3. Experimental

Chemicals: GNF were purchased from Pyrograf Products Inc (PR19, chemical vapor deposition), USA. $Co@C_n$ was purchased from Turbobeads LLC, USA. All other reagents and solvents were purchased from Sigma-Aldrich (UK) and used without further purification.

The glassware required to perform the experiments was thoroughly cleaned with 'aqua regia' (concentrated hydrochloric and nitric acids (3:1)) and rinsed with deionised water prior to use.

Synthesis of $(Co@C_n)$/GNF: GNF (15 mg, annealed at 450 °C in air for 1 hour prior to use) in hexane (20 mL) and $Co@C_n$ (1.5 mg, corresponding to 10 % by wt. Co in the final $(Co@C_n)$/GNF material) in hexane (5 mL) were dispersed separately using an ultrasonication bath (3 L Ultrasonic cleaner, Agar Scientific, 100 W and 40 kHz) for 10 min. Once dispersed

the $Co@C_n$ hexane suspension was slowly added to the GNF dispersion in small portions (0.2 mL) whilst being treated with ultrasonic waves, the resultant dispersion was then sonicated for a further 10 min. Separation of resultant $(Co@C_n)$/GNF as a black powder was achieved by applying a magnet to the outside of the vial and decanting the hexane solvent.

Synthesis of $(Fe@C_n)$/GNF: ferrocene (5 mg, corresponding to 10 % by wt. Fe in the final $(Fe@C_n)$/GNF) was combined with GNF (15 mg, annealed at 450 °C for 1 hour prior to use) in a Pyrex tube and sealed under vacuum (10^{-6} bar) using a vacuum pump. The material was then heated at 350 °C for 1 day, and the temperature was then increased to 500 °C for a further day. The sample was then cooled and opened to yield the $(Fe@C_n)$/GNF material as black powder.

Synthesis of PdNPs@GNF-1: $Pd(acac)_2$ (0.22 mg, corresponding to 0.5 % by wt. Pd in the final PdNPs@GNF-1) was combined with GNF (15 mg, annealed at 450 °C for 1 hour prior to use) in a Pyrex tube and sealed under vacuum (10^{-6} bar) using a vacuum pump and heated at 150 °C for 3 days. After 3 days, the sample inside the Pyrex tube was cooled by immersing in an ice bath. The sample was then removed from the Pyrex tube and sealed in a separate Pyrex tube under argon atmosphere and heated at 550 °C for 3 hours. The final material was then cooled to give PdNPs@GNF-1 as black powder.

Synthesis of PdNPs@GNF-2: GNF (15 mg, annealed at 450 °C for 1 hour prior to use) were dispersed in $CHCl_3$ (2 mL) using ultrasound for 10 min. A solution of tris(dibenzylideneacetone)dipalladium(0)-chloroform adduct ($Pd_2(dba)_3.CHCl_3$) (0.375 mg, corresponding to a 0.5 % by wt. of Pd in the final PdNPs@GNF-2 material) in $CHCl_3$ (1 mL) was then slowly added to the GNF dispersion in small portions (0.1 mL) whilst being treated with ultrasonic waves and stirred at 40 °C for 4 hours until the solution became colourless. PdNPs@GNF was then separated from the reaction mixture by filtration and washed repeatedly with acetone (20 mL) using a 0.2 µm PTFE membrane filter to remove free dibenzylideneacetone (dba) to yield the PdNPs@GNF-2 material as black powder.

Synthesis of PtNPs@GNF-1: Pt(acac)$_2$ (0.30 mg, corresponding to a 1 % by wt. of Pt in the final PtNPs@GNF-1 material) was combined with GNF (15 mg, annealed at 450 °C for 1 hour prior to use) in a Pyrex tube and sealed under vacuum (10^{-6} bar) using a vacuum pump and heated at 170 °C for 3 days. After 3 days, the sample was cooled by immersing in an ice bath and then removed from the Pyrex tube and sealed in a separate Pyrex tube under an argon atmosphere and heated at 550 °C for 3 hours. The final PtNPs@GNF-1 was then recovered as black powder.

Synthesis of PtNPs@GNF-2: GNF (15 mg, annealed at 450 °C for 1 hour prior to use) were dispersed in CHCl$_3$ (2 mL) using ultrasound for 10 min. A solution of tris(dibenzylideneacetone)platinum(0) (Pt(dba)$_3$) (0.69 mg, corresponding to a 1 % by wt. of Pt in the final PtNPs@GNF-2 material) in CHCl$_3$ (1 mL) was then slowly added to the GNF dispersion in small portions (0.1 mL) whilst being treated with ultrasonic waves and stirred at 70 ° C for 1 day until the solution became colourless. PtNPs@GNF was then separated from the reaction mixture by filtration and washed repeatedly with acetone (20 mL) using a 0.2 µm PTFE membrane filter to remove free dibenzylideneacetone (dba) and obtain the final PtNPs@GNF-2 material as black powder.

Synthesis of Magnetic PdNPs@((Co@C$_n$)/GNF): PdNPs@GNF-2 (15 mg) in hexane (20 mL) and Co@C$_n$ (1.5 mg) in hexane (5 mL) were dispersed separately using ultrasound for 10 min. The Co@C$_n$ hexane suspension was then added to the GNF dispersion in small portions (0.1 mL) whilst being treated with ultrasonic waves, the resultant dispersion was then sonicated for a further 10 min. The separation of catalyst from the solution was controlled by an external magnet (0.1 T) to give PdNPs@((Co@C$_n$)/GNF) as black powder.

Synthesis of Magnetic PdNPs@((Fe@C$_n$)/GNF): (Fe@C$_n$)/GNF (15 mg) was dispersed in CHCl$_3$ (2 mL) using ultrasound for 10 min. Once GNF was dispersed, Pd$_2$(dba)$_3$.CHCl$_3$ (0.34 mg) dissolved in CHCl$_3$ (1 mL) were added to GNF dispersion in small portions (0.1 mL) whilst

being treated with ultrasonic waves and stirred at 40 C° for 4 h until the solution became colourless. PdNPs@GNF was then separated from the reaction mixture by filtration using a 0.2 µm PTFE membrane filter and washed repeatedly with acetone (20 mL) to remove the free dibenzylideneacetone and give PdNPs@((Fe@C$_n$)/GNF) as black powder.

Synthesis of Magnetic PtNPs@((Co@C$_n$)/GNF): PtNPs@GNF-1 (15 mg) in hexane (20 mL) and Co@C$_n$ (1.5 mg) in hexane (5 mL) were dispersed separately using ultrasound for 10 min. Once dispersed the Co@C$_n$ in hexane were slowly added to GNF dispersion in small portions whilst being treated with ultrasonic waves, the resultant dispersion was then sonicated for a further 10 min. Separation of the resultant PtNPs@((Co@C$_n$)/GNF) as black powder was achieved by applying a magnetic field (0.1 T) to the outside of the vial and decanting the hexane solvent.

Magnetic PtNPs@((Fe@C$_n$)/GNF): Pt(acac)$_2$ (0.3 mg, 1% by wt. Pd) was combined with (Fe@C$_n$)/GNF (15 mg) in a Pyrex tube, sealed under vacuum (10^{-6} bar) using a vacuum pump and heated at 170 °C for 3 days. The sample inside the Pyrex tube was then cooled by immersing in an ice bath. The sample was removed from the Pyrex tube and sealed in a separate Pyrex tube under an argon atmosphere and heated at 550 °C for 3 hours. PtNPs@((Fe@C$_n$)/GNF) was then isolated as black powder.

Reduction of nitrobenzene using a high pressure H$_2$ glass reactor: The selected catalyst (10 mg, equivalent to 0.00051 mmol of metal nanoparticles) and an ethanol (0.5 mL) solution of nitrobenzene (0.78 mmol) were stirred in a high-pressure reactor (10 mL volume). The reactor volume was then degassed thoroughly with H$_2$ for 15 min. The reactor was then sealed and pressurised with H$_2$ (8 bar) and left for 30 minutes at room temperature. At the end of the reaction, the reactor was slowly depressurized and analysed via ^{1}H NMR spectroscopy using CDCl$_3$ solvent. *Nitrobenzene (Ph-NO$_2$):* ^{1}H NMR (300 MHz, 297 K, CDCl$_3$, δ, ppm): 8.20-8.17 (m, 2H; CH-CH), 7.69-7.63 (m, 1H;CH, 7.53-7.48 (m, 2H; CH-CH). N-phenylhydroxylamine

(Ph-NHOH): ^{1}H NMR (300 MHz, 297 K, CDCl$_3$, δ, ppm): 7.23-7.18 (m, 2H; CH-CH), 6.95-6.93 (d, J = 7.54 Hz, 2H; CH-CH), 6.90-6.85 (m, 1H; CH). Aniline (Ph-NH$_2$): ^{1}H NMR (300 MHz, 297 K, CDCl$_3$, δ, ppm): 7.13-7.07 (t, J = 7.86 Hz, 2H, CH-CH), 6.73-6.69 (m, 1H; CH), 6.68-6.64 (m, 2H; CH-CH).

Characterisation techniques: ^{1}H NMR spectra were recorded using a Bruker DPX300 NMR spectrometer. ^{1}H NMR spectra were taken in CDCl$_3$ and were referenced to residual trimethysilane (TMS) (0 ppm) and reported as follows: chemical shift, multiplicity (s = singlet, d = doublet, t = triplet, dd = doublet of doublet, m = multiplet). HRTEM analysis was performed on a JEOL 2100 Field emission gun microscope with an information limit of 0.12 nm at 100 kV. Samples for HRTEM analysis were prepared by dispersing the materials in HPLC grade iso-propanol using ultra-sonication, then drop casting the resultant suspension onto a lacey carbon film coated copper grid. TGA analysis was performed on a TA Instruments TGA-SDTQ600 analyser. Samples for TGA analyses were heated in air up to 1000 °C with a heating rate of 10 °C/min. The powder X-ray diffraction patterns were obtained using a PANanalytical X'Pert PRO diffractometer equipped with a Cu-Ka radiation source (λ= 1.542) operating at 40 kV and 40 mA, with 0.05252° step size and a step time of 5925.18 seconds. Surface area analysis was performed using the Brunauer–Emmett–Teller (BET) method based on adsorption data in the relative pressure (P/Po) range 0.02 to 0.22 by measuring nitrogen sorption isotherms of the samples (50 mg) at -196 °C on a Micromeritics ASAP 2020 sorptometer. Before analysis, the samples were evacuated for 12 h at 200 °C under vacuum. The pore size distributions were obtained from a Non-Local Density Functional Theory (NLDFT) method using nitrogen-sorption data.

UV–Visible spectroscopy measurements: (Co@C$_n$)/GNF (10 mg) and (Fe@C$_n$)/GNF (10 mg) were suspended in hexane (10 mL) by stirring at 500 rpm using a magnetic stirrer for 2 min and

then a magnetic field was applied for a set periods of time (10, 30, 60 and 90 seconds). For example, after applying a magnetic field for 10 s, 2 mL of solution were taken from the magnetically separated solution using a micro pipette then analysed by UV–Vis spectroscopy between 350–700 nm (wavelength step: 1 nm, scan speed: 240 nm min^{-1}) using a Perkin Elmer Lambda 11 spectrophotometer. The 2 mL solution was then returned to the starting solution and the solution was re-dispersed and the same procedure was repeated.

Magnetic measurements on (Co@C$_n$)/GNF and (Fe@C$_n$)/GNF were carried out in a commercial Quantum Desing MPMS-XL5 Superconducting Quantum Interference Device (SQUID) magnetometer. Samples were carefully prepared using a plastic capsule with a negligible diamagnetic contribution. For both samples variable-temperature (1.8─300 K, with 0.1 T applied field) and field dependent (at 2 K and 300 K with a maximum field of 5 T) magnetisation measurements were carried and compared by dividing the magnetic signal per mass of the measured sample.

ICP-OES measurements: PdNPs@GNF-2 and PtNPs@GNF-1 samples (3 x 2 mg), were burned in a boiling tube using a bunsen burner to fully oxidise and hence remove the GNF. The remaining residual metal was then digested in acid (1 mL, aqua regia,) at room temperature using ultra-sonication for 1 h and the resultant solution was diluted with ultrapure water to make a dilute aqua regia solution (10 % by volume in water). ICP-OES was used to determine the Pd and Pt % loadings of the solutions, respectively using a Perkin Elmer, Optima 2000 DV ICP-OES with S10 autosampler with an axial detection method at wavelengths of 340.458 nm for Pd and 214.423 nm for Pt. Calibration Pd and Pt solutions (0.1, 0.2, 0.5, 1 and 5 mg L^{-1}) were prepared using a Pd standard (Sigma Aldrich) and a Pt standard (VWR Chemicals) and aqua regia (10 % by volume in water), and gave a linear plot with an R coefficient of 0.999999. Blanks showed 0.00 mg L^{-1} of Pd and Pt, respectively. Corrected concentrations of Pd and Pt

were then measured as number of mg of Pd and Pt per litre for each sample and correlated to Pd and Pt % loadings.

Catalyst recovery by applying a magnetic field: After each experimental cycle, the catalyst mixed with reaction products were extracted into ethanol (5 mL) and then applied magnetic field. As the catalyst accumulated on the wall of reaction vessel, the solution mixture was easily separated from the catalyst using a pipette. Ethanol (5 mL) was then added to the catalyst and the same procedure was repeated until no signs of starting materials or products could be observed by ^{1}H NMR. The catalyst was then left to dry at room temperature.

Catalyst recovery by filtration: After each experimental cycle, the catalyst, mixed with reaction products, was extracted into ethanol (5 mL) and then washed with ethanol (20 mL) using a filtration assembly and a PFTE membrane followed by drying at ambient conditions. The washings were repeated until no signs of starting materials or products could be observed by ^{1}H NMR. The catalyst was then collected from the filtration membrane using a spatula.

Supporting Information
Supporting Information is available from the Wiley Online Library.

References

[1]   S. Iijima, Nature, **1991**, 354.

[2]   M. S. Dresselhaus, G. Dresselhaus, A. Jorio, Annu. Rev. Mater. Res., **2004**, 34, 247-278.

[3]   S. A. Hodge, M. K. Bayazit, K. S. Coleman, M. Shaffer, Chem. Soc. Rev., **2012**, 41, 4409-4429.

[4]   A. Mamalis, Precis. Eng., **2004**, 28, 16-30.

[5]   M. Terrones, Int. Mater. Rev., **2004**, 49, 325.

[6]   M. S. Dresselhaus, G. Dresselhaus, P. Avouris, Carbon nanotubes: Synthesis, structure, properties, and applications, Springer, New York, **2001**.

[7]   G. A. Rance, D. H. Marsh, S. J. Bourne, T. J. Reade, A. N. Khlobystov, ACS Nano, **2010**, 4, 4920-4928.

[8]   M. Daenen, R. D. De Fouw, B. Hamers, P. G. A. Janssen, K. Schouteden, M. A. J. Veld, The Wondrous World of Carbon Nanotubes 'a review of current carbon nanotube technologies'. Eindhoven University of Technology, **2003**, 1-96.

[9]   H. Chu, L. Wei, R. Cui, J. Wang, Y. Li, Coord. Chem. Rev., **2010**, 254, 1117-1134.

[10]   A. N. Khlobystov, ACS Nano, **2011**, 5, 9306-9312.

[11]   P. Serp, J. L. Figueiredo, Carbon materials for catalysis, Wiley, **2009**, 56.

[12]   G. G. Wildgoose, C. E. Banks, R. G. Compton, Small, **2006**, 2, 182-193.

[13]   W. A. Solomonsz, G. A. Rance, B. J. Harris, A. N. Khlobystov, Nanoscale, **2013**, 5, 12200-12205.

[14]   M. J. Ledoux, R. Vieira, C. Pham-Huu, N. Keller, Catalysts. J. Catal., **2003**, 216, 333.

[15]   T. W. Chamberlain, J. H. Earley, D. P. Anderson, A. N. Khlobystov, R. A. Bourne, Chem. Commun., **2014**, 50, 5200-5202.

[16]   P. Serp, M. Corrias, P. Kalck, Appl. Catal. A, **2003**, 253, 337-358.

[17]   S. A. Miners, G. A. Rance, A. N. Khlobystov, Chem. Commun., **2013**, 49, 5586-5588.

[18]   W. A. Solomonsz, G. A. Rance, M. Suyetin, A. La Torre, E. Bichoutskaia, A. N. Khlobystov, Chem. Eur. J., **2012**, 18, 13180-13187.

[19]   M. A. Lebedeva, T. W. Chamberlain, A. Thomas, B. E. Thomas, C. T. Stoppiello, E. Volkova, M. Suyetind, A. N. Khlobystov, Nanoscale, **2016**, 8, 11727-11737.

[20]   X. Pan, Z. Fan, W. Chen, Y. Ding, H. Luo, X. Bao, Nat. Mater., **2007**, 6, 507-511.

[21] B. Cornelio, A. R. Saunders, W. A. Solomonsz, M. Laronze-Cochard, A. Fontana, J. Sapi, A. N. Khlobystov and G. A. Rance, J. Mater. Chem. A, **2015**, 3, 3918-3927.

[22] W. A. Solomonsz, G. A. Rance and A. N. Khlobystov, Small, **2014**, 10, 1866-1872.

[23] G. A. Rance, W. A. Solomonsz and A. N. Khlobystov, Chemm. Commun., **2013**, 49, 1067-1069.

[24] M. Aygün, C.T. Stoppiello, M. A. Lebedeva, E. F. Smith, M. D. C. Gimenez-Lopez, A. N. Khlobystov, T. W. Chamberlain, J. Mater. Chem. A, **2017**, 5, 21467-21477.

[25] M. Gimenez-Lopez, A. Kurtoglu, D. A. Walsh, A. N. Khlobystov, Adv. Mat., 2016, 28, 9103-9108.

[26] X. Pan, X. Bao, Chem. Commun., **2008**, 6271-6281.

[27] X. Pan, X. Bao, Acc. Chem. Res., **2011**, 44, 553-562.

[28] A. Hutten, D. Sudfeld, I. Ennen, G. Reiss, W. Hachmann, U. Heinzmann, K. Wojczykowaki, P. Jutzi, W. Saikaly, G.J. Thomas. Biotechnol., **2004**, 112, 47.

[29] A. H. Lu, W. Schmidt, N. Matoussevitch, H. Bönnemann, B. Spliethoff, B. Tesche, E. Bill, W. Kiefer, F. Schüth, Angew. Chem., **200**4, 116, 4403.

[30] H. Jia, Y. Lian, M. Ishitsuka, T. Nakahodo, Y. Maeda, T. Tsuchiya, T. Wakahara, T. Akasaka, Sci. Technol. Adv. Mater., **2005**, 6, 571-581.

[31] L. M. Rossi, N. J. S. Costa, F. P. Silva, R. V. Gonçalves, Nanotechnol. Rev., **2013**, ,2, 597-614.

[32] J. Govan, Y. K. Gun'ko, Nanomaterials, **2014**, 4, 222–241.

[33] L. M. Rossi, N. J. S. Costa, F. P. Silva, R. Wojcieszak, Green. Chem., **2014**, 16, 2906-2933.

[34] M. D. Lekgoathi, W.G. Augustyn, J. Heveling, J. Nanosci. Nanotechnol., **2011**, 11, 7001-7005.

[35]   H. M. Torres Galvis, J. H. Bitter, C. B. Khare, M. Ruitenbeek, A. I. Dugulan, K. P. de Jong, Science, **2012**, 335, 835.

[36]   M. Melchionna, A. Beltram, A. Stopin, T. Montini, R. W. Lodge, A. N. Khlobystov, D. Bonifazi, M. Prato, P. Fornasiero, Appl. Catal., B, **2018**, 227, 356-365.

[37]   R. N. Grass, W. J. Stark, J. Mater. Chem., **2006**, 16, 1825-1830.

[38]   I.K. Herrmann, R. N. Grass, D. Mazunin, W. J. Stark, Chem. Mater., **2009**, 21, 3275-3281.

[39]   Y. Deng, Y. Cai, Z. Sun, J. Liu, J. Wei, W. Li, C. Liu, Y. Wang, D. Zhao, J. Am. Chem. Soc., **2010**, 132, 8466-8473.

[40]   L. Zhang, Li. Pinhua, L. Hongji, L. Wang, Catal. Sci. Technol., **2012**, 2, 1859-1864.

[41]   A. H. Lu, E. L. Salabas, F. Schüth, Angew. Chem., Int. Ed., **2007**, 46, 1222-1244.

[42]   S. C. Tsang, V. Caps, I. Paraskevas, D. Chadwick and D. Thompsett, Angew. Chem., Int. Ed., **2004**, 43, 5649-5649.

[43]   Z. Xu, H. Li, G. Cao, Z. Cao, Q. Zhang, K. Li, X. Hou, W. Lia, W. Cao, J. Mater. Chem., **2010**, 20, 8230-8232.

[44]   M. Rossier, F. M. Koehler, E. K. Athanassiou, R. N. Grass, B. Aeschlimann, D. Günther, W. J. Stark, Mater. Chem., **2009**, 19, 8239-8243.

[45]   S. Wittmann, A. Schätz, R. N.Grass, W. J. Stark, O. Reiser, Angew. Chem. Int. Ed., **2010**, 49, 1867-1870.

[46]   G.U. Sumanasekera, B.K. Pradhan, H.E. Romero, K.W. Adu, P.C. Eklund, Phys. Rev. Lett., **2002**, 89, 166801.

[47]   I. K. Herrmann, M. Urner, F. M. Koehler, M. Hasler, B. Roth-Z'Graggen, R. N. Grass, U. Ziegler, B. Beck-Schimmer, W. Stark, Small, **2010**, 6, 1388-1390.

[48]   A. Schätz, T. R. Long, R. N. Grass, W. J. Stark, P. R. Hanson, O. Reiser, Chem. Mater., **2010**, 20, 4323-4328.

[49]   A. Schätz, R. N. Grass, Q. Kainz, W. J. Stark, O. Reiser, Chem. Mater., **2010**, 22, 305-310.

[50]   B. K. T. Kenneth, C. Singh, M. Chhowalla, W.I. Milne, Encycl. Nanosci. Nanotechnol., **2004**, 1, 665-686.

[51]   R. Saito, G. Dresselhaus, M. S. Dresselhaus, Physical Properties of Carbon Nanotubes, Imperial College Press, **1998**.

[52]   A. W. Hull, Phys. Rev., **1917**, 10, 661-696.

[53]   A. Combessis, C. Mazel, M. Maugin, L. Flandin, J. Appl. Polym. Sci., **2013**, 130, 1778-1786.

[54]   S. H. Jeong, K. K. Kim, S. J. Jeong, K. H. An, S. H. Lee, Y. H. Lee, Synth. Met., **2007**, 157, 570–574.

[55]   I. M. L. Billas, A. Châtelain,W.A. de Heer, Science, **1994**, 265, 1682-1684.

[56]   R. S. Downing, P. J. Kunkeler, H. van Bekkum, Catal. Today, **1997**, 37, 121-136.

[57]   S. L. Karwa, K. A. Rajadhyaskha, Ind. Eng. Chem. Res., **1987**, 26, 1746-1750.

[58]   E.A. Gelder, S.D. Jackson, C.M. Lok, Catal. Lett., **2002**, 84, 205-208.

[59]   C. H. Li, Z. X. Yu, K. F. Yao, S. F. Ji, J. Liang, J. Mol. Catal. A, **2005**, 226, 101-105.

[60]   P. Sangeetha, K. Shanthi, K.S. Rama Rao, B. Viswanathan, P. Selvam, Appl. Catal. A Gen., **2009**, 353, 160-165.

[61]   Y. Takenaka, T. Kiyosu, J. Choi, T. Sakakuraa, H. Yasuda, Green Chem., **2009**, 11, 1385-1390.

[62]   F. A. Westerhaus, R. W. Jagadeesh, G. Wienho, M. Pohl, J. Radnik, A. Surkus, J. Rabeah, K. Junge, H. Junge, M. Nielsen, A. Bruckner, M. Beller, Nat. Chem., **2013**, 5, 537-543.

[63]   M. Shokouhimehr, T. Kim, J.S. Woojoo, S. Kwangsoo, Y. Jang, B. H. Kim, J. Kim, T. Hyeon, Appl. Catal., A, **2014**, 476, 133-139.

[64]   M. Turáková, M. Králik, P. Lehocky, P. Pikna, M. Smrcová, D. Remeteiová, A. Hudák, Appl. Catal., A,**2014**, 476, 103-112.

[65]   R. B. N. Baig, R. S. Varma, ACS Sustainable Chem. Eng., **2014**, 2, 2155-2158.

[66]   E. O. Pentsak, A. S. Kashin, M. V. Polynski, K. O. Kvashnina, P. Glatzelc, V. P. Ananikov, Chem. Sci., **2015**, 6, 3302

[67]   A.W. Hull, W.P. Davey, Phys. Rev., **1921**, 17, 571-587.

[68]   E. O. Pentsak , V. P. Ananikov, Russ. Chem. Bull., **2014**, 63, 2560.

[69]   H. E. Swanson, E., Tatge, Standard X-ray diffraction powder patterns I, National Bureau of Standards, U.S., Circular, **1953**.

[70]   Z. Haber. Elektrochem., **1898**, 4, 506-513.

[71]   E.A. Gelder, S.D. Jackson, C.M. Lok, Chem. Comm., **2005**, 4, 522-524.

[72]   A. Corma, P. Concepcion, P. Serna, Angew. Chem. Int. Ed., **2007**, 46, 7266-7269.

[73]   M. Turákováa, T. Salmi, K. Eränenc, J. Wärnåc, D. Y. Murzinc, M. Králik, Appl. Catal., A, **2015**, 499, 66-76.